Am J Transl Res 2026;18(5):4577-4592
www.ajtr.org /ISSN:1943-8141/AJTR0172582

Original Article

Brazilin induces apoptosis and autophagy in human glioblastoma cells via the PI3K/AKT/mTOR signaling pathway

Minghua Shang[1,2,3], Jinyi Yu[4], Xingang Li[1,2]

[1]Department of Neurosurgery, Qilu Hospital, Cheeloo College of Medicine and Institute of Brain and Brain-Inspired Science, Shandong University, Jinan 250012, Shandong, China; [2]Jinan Microecological Biomedicine Shandong Laboratory and Shandong Key Laboratory of Brain Health and Function Remodeling, Jinan 250117, Shandong, China; [3]Department of Neurosurgery, The Affiliated Yantai Yuhuangding Hospital of Qingdao University, Yantai 264000, Shandong, China; [4]Department of Ophthalmology, The Affiliated Yantai Yuhuangding Hospital of Qingdao University, Yantai 264000, Shandong, China

Received March 11, 2026; Accepted May 25, 2026; Epub May 25, 2026; Published May 30, 2026

Abstract: Objectives: Brazilin (BZ), an active isoflavonoid from Chinese herbs, exhibits antitumor properties. This study investigated its antitumor efficacy and molecular mechanisms in human glioblastoma (GBM) cells. Methods: GBM cell proliferation and viability were assessed using xCELLigence RTCA eSight™, cell counting kit-8, 5-ethynyl-2'-deoxyuridine, live/dead staining, and colony formation assays. Migration and invasion were evaluated by Transwell, three-dimensional invasion, and wound healing assays. Apoptosis was analyzed by flow cytometry, and target protein expression by western blot. A xenograft model was established by subcutaneous injection of P3 cells into nude mice, followed by BZ treatment at different concentrations. Results: BZ significantly inhibited GBM cell proliferation and viability in time- and dose-dependent manners. It also suppressed cell invasion and migration dose-dependently. Apoptosis rates in U251, P3, and LN229 cells increased significantly after BZ treatment. Accordingly, BZ upregulated the apoptosis-related proteins B-cell lymphoma 2 (BCL-2)-associated X protein and cleaved poly (ADP-ribose) polymerase-1, as well as the autophagy-related protein LC3B, while downregulating BCL-2 and sequestosome 1. Phosphorylated phosphoinositide 3-kinase (PI3K), protein kinase B (AKT), and mammalian target of rapamycin (mTOR) levels were reduced in BZ-treated U251 and LN229 cells. Finally, BZ inhibited the growth of orthotopic xenografts from luciferase-expressing P3 cells in mice. Conclusions: BZ induces apoptosis and autophagy in GBM cells via the PI3K/AKT/mTOR signaling pathway, suggesting its potential as a novel therapeutic agent for GBM patients.

Keywords: Glioblastoma, brazilin, apoptosis, autophagy, PI3K/AKT/mTOR signaling pathway

Introduction

Human glioblastoma (GBM) is the most prevalent and aggressive primary brain tumor in the central nervous system [1]. Currently, the standard treatment regimen for GBM is maximal surgical resection combined with the first-line chemotherapy drug temozolomide and radiotherapy [2]. The mean survival time of patients with GBM after surgery is 12-15 months, and the 5-year survival rate is less than 5% [3, 4]. However, due to the limited number of drugs entering the central nervous system, the high invasiveness of GBM cells, and the presence of stem cell-like tumor cells, GBM is resistant to chemotherapy, radiotherapy, and immunotherapy [5]. Therefore, there is an urgent need for new effective therapeutic strategies to inhibit the growth and metastasis of GBM.

Traditional Chinese medicine is an important resource for treating human cancer. For centuries, many traditional Chinese medicines have been used to treat human diseases. For example, brazilin (BZ), a natural isoflavone derived from plants such as Caesalpinia sappan and Haematoxylum braziletto, has garnered attention for its potential medicinal properties, including inhibition of oxidative stress [6] and inflammation [7], antibacterial effects [8], and anti-cancer [9], anti-diabetic [10], neuroprotective [11], and other activities [12]. According to

https://doi.org/10.62347/DAHL4962

recent research, autophagy plays important roles in the growth, apoptosis, and proliferation of cancer cells [13-15]. Autophagy is a lysosome-dependent cellular degradation program during which eukaryotic cells deliver abnormal proteins and degraded organelles to the lysosomal degradation pathway. Autophagy can be divided into three main types: macroautophagy, microautophagy, and chaperone-mediated autophagy [16-18]. Among them, macroautophagy has been the most widely studied type of autophagy worldwide. Therefore, we focused on macroautophagy (hereafter referred to as autophagy) in this study. Autophagosomes fuse with lysosomes to form autolysosomes, and the cargo is degraded [19, 20]. The current relationships between autophagy and cell death include (1) the simultaneous occurrence of autophagy and apoptosis, (2) autophagic cell death, and (3) autophagy-mediated cell death [21]. Autophagy-induced cell death is also termed preautophagy-triggered cell death [22]. Notably, studies have shown that other isoflavones can induce autophagy [23-25], raising the question of whether BZ shares this property in the context of GBM. Even though numerous studies have demonstrated that BZ exerts potent anti-tumor effects on the progression of different types of tumors, whether BZ regulates GBM development through apoptosis and autophagy remains unclear.

We investigated the effects of BZ on GBM cells in vivo and in vitro. We experimentally demonstrated that BZ exerts potent anti-tumor effects on GBM cells mainly through apoptosis, autophagy, and the phosphoinositide 3-kinase (PI3K)/protein kinase B (AKT)/mammalian target of rapamycin (mTOR) signaling pathway, one of the major pathways involved in GBM pathology.

Materials and methods

Experimental animals and ethics statement

Male BALB/c nude mice (approximately 4 weeks old) were obtained from the Nanjing Biomedical Research Institute of Nanjing University (Nanjing, China) and maintained in the animal facility of the neurosurgery laboratory of Qilu Hospital, Shandong University under pathogen-free conditions. All procedures were approved by the Ethics Committee and the Laboratory Animal Research Centre of Qilu Hospital, Shandong University (Approve number: DWLL-202500500).

Cell lines and culture

The human GBM cell lines U251 and LN229 were purchased from the Chinese Academy of Sciences Cell Bank (Shanghai, China) and authenticated by short tandem repeat profiling. All human GBM cells were cultured in Dulbecco's modified Eagle's medium (MACGENE Biotechnology Ltd; Beijing, China) supplemented with 10% foetal bovine serum (Biological Industries, Israel), streptomycin (100 U/ml), and penicillin (100 U/ml). The primary human GBM cell line P3 was kindly provided by Professor Rolf Bjerkvig from the University of Bergen and cultured in neurobasal medium (21103049; Thermo Fisher Scientific) supplemented with 2% B27 (A3653401; Thermo Fisher Scientific), 1% L-glutamine (A400022-5301; Thermo Fisher Scientific), 1% penicillin/streptomycin (P1400; Solarbio), 20 ng/ml epidermal growth factor (AF-100-15; Peprotech; Rocky Hill, NJ, USA), and 20 ng/ml basic fibroblast growth factor (100-18B; Peprotech). All the cells were incubated in a humidified chamber with 5% CO_2 at 37°C.

xCELLigence RTCA eSight™ viability assay

Dynamic monitoring of U251, LN229 and P3 cell viability was performed with the xCELLigence RTCA eSight™ system (Agilent Biosciences, Hangzhou, China). GBM cells were seeded in 96-well plates at the optimal cell density and treated with or without 40 μM BZ for viability assessment. Cell growth curves were recorded on the xCELLigence RTCA eSight™ system in real time with measurements taken every 2 hours.

Cell viability assays

GBM cells were cultured under optimal conditions, and their concentrations were adjusted to evaluate cell proliferation. U251, LN229 and P3 cells were seeded into 96-well plates at a density of 3000 cells per well and incubated for 24, 48, and 72 h. After 24 h, cell adhesion was confirmed, and the original medium was gently discarded. The treatment groups received medium supplemented with BZ at concentrations of 15, 30, 45, 60, 75, 90, and 105 μM. The control group did not receive BZ. After incubation, cell counting kit-8 (CCK-8, CK04-500; Dojindo Laboratories; Kumamoto, Japan) solution was added, and the cells were incubated

for an additional 4 h at 37°C. The absorbance was then measured at 450 nm using a microplate reader. Each treatment was performed in triplicate. The experiments were conducted with five replicates and independently repeated three times.

Cell proliferation assay

Cells were cultured for 24 h in 24-well plates with 5×10^4 cells/well. The 5-ethynyl-2'-deoxyuridine (EdU) incorporation assay kit (C103103; RiboBio; Guangzhou, China) used according to the manufacturer's instructions. The EdU solution was mixed with complete medium and added to each group of cells. Cells were fixed with 4% paraformaldehyde (pH 7.4) for 30 minutes and then neutralized with glycine solution (2 mg/mL) for 5 minutes. Cells were washed with phosphate-buffered saline (PBS) and stained with the anti-EdU working solution at room temperature for 30 minutes. After that, 4',6-diamidino-2-phenylindole (DAPI) staining solution was added and incubated for 10 minutes. Cells stained with DAPI (blue) and EdU (red) were observed using an FSX100 microscope (Olympus, Tokyo, Japan) in the dark. EdU-positive cells (%) = (number of EdU-positive cells/total number of DAPI-stained cells) × 100%.

Colony formation assay

U251 and LN229 cells were seeded in a 6-well cell culture plate (200 cells per well) and allowed to adhere overnight. The cells were then treated with various concentrations of BZ (20, 40 μM) or a control. Throughout the experiment, the medium was replaced every 3 days with fresh medium containing the corresponding concentration of BZ. After two weeks, the colonies were fixed with 4% paraformaldehyde for 15 minutes and rinsed three times with PBS. Afterwards, the cells were stained with 0.5% crystal violet for approximately 15 minutes. Finally, images were obtained, and the number of colonies was counted.

Wound healing assay

U251 and LN229 cells were seeded into 6-well plates containing serum-free growth medium and cultured. After 24 h of incubation, a scratch was manually made in each well using a 100 μL pipette tip. The wells were gently washed with PBS to remove cell debris and then incubated with medium containing BZ (0, 20, or 40 μM) at 37°C. Images were obtained under a microscope at 24 h and 48 h after treatment, and the wound width (distance between the two cell edges) was statistically analyzed.

Transwell assay

Invasion was measured using the Transwell Matrigel assay. GBM cells were seeded into 6-well plates and treated with BZ (0, 20, or 40 μM) for 48 h. After treatment, the cells were trypsinized, counted, and resuspended in serum-free medium, then plated into BD Biocoat Matrigel Invasion Chambers (8 μM pore size; BD Biosciences). The chemoattractant in the bottom wells was medium supplemented with 10% foetal bovine serum. Invading cells were fixed after 24 h, stained with crystal violet, counted in 4 random fields with a microscope, and statistically analyzed.

Cell invasion in three-dimensional (3D) culture

GBM cells (3×10^3) were seeded into each well of 3D Culture Qualified 96-well spheroid formation plates (Trevigen, Gaithersburg, MD, USA) with 100 μL of medium and cultured at 37°C in a 5% CO_2 humidified incubator for 72 h. After 72 h, the cells formed tumor spheroids. The plates were placed on ice for 15 minutes, and 50 μL of invasion matrix (Trevigen, 3500-096-K, Cultrex) was added to each well. The plates were centrifuged at 300×g at 4°C for 5 minutes and then incubated at 37°C for 1 h. Medium (100 μL) containing different concentrations of BZ was added to each well. Images of the spheroids were captured every 24 h using bright-field microscopy. Images acquired at 96 h were analyzed using ImageJ software.

Live/dead viability/cytotoxicity assay

Human GBM cells were treated with different concentrations of BZ and then stained using the live/dead viability/cytotoxicity kit (Invitrogen, USA) for viability assessment. Cells were washed three times with 1 mL of ice-cold 1× PBS. Then, 100 μL of live/dead mix (containing 2 μM calcein AM and 4 μM ethidium homodimer-1 in 1 mL of 1× PBS) was added to each well. After incubation for 15 minutes at 37°C, live cells were stained green (calcein AM), and dead cells were stained red (ethidium homodimer-1). Cells were imaged using Alexa Fluor

488 and EthD-1 filters under a Carl Zeiss Axio Z1 live imaging microscope.

Apoptosis assays

We used an Annexin V-fluorescein isothiocyanate/propidium iodide apoptosis detection kit to assess the apoptosis rate of GBM cells. Briefly, 1×10^5 untreated or BZ-treated cells were collected. The cells were stained with 5 μL of Annexin V-fluorescein isothiocyanate apoptosis detection kit (BD Biosciences, La Jolla, CA, USA) and 10 μL of propidium iodide, then incubated for 15 minutes in the dark at room temperature. The results were analyzed using FlowJo software (Tree Star, Ashland, OR, USA).

Autophagy assays

To detect autophagy, cells were transfected with a green fluorescent protein (GFP)-mCherry-light chain 3 (LC3B) vector (Guangzhou Aiji Biotechnology Co., Ltd., Guangzhou, China) according to the manufacturer's protocol. Following a change of medium, the virus-transfected cells were treated with or without BZ. The cells were then fixed with 4% paraformaldehyde for 30 min and stained with DAPI (1 μg/ml) for 15 min at room temperature. Immunofluorescence images were captured using a confocal microscope (Leica, SP8; Solms, Germany). Co-localization of GFP and mCherry (yellow) indicated autophagosomes, while mCherry alone (red) indicated autophagolysosomes.

Western blot (WB) analysis

U251 and LN229 cells were treated with 0, 20, and 40 μM BZ for 48 h and then lysed in radioimmunoprecipitation assay buffer (P0013C, Beyotime, Haimen, China). The lysates were subsequently centrifuged, and the protein concentration was determined using a bicinchoninic acid assay kit (Beyotime, Shanghai, China). Equal amounts of protein from each sample were separated by sodium dodecyl sulfate-polyacrylamide gel electrophoresis and transferred to polyvinylidene fluoride membranes. The membranes were blocked with 5% non-fat milk for 2 h at room temperature and then incubated with primary antibodies overnight at 4°C. After the membranes were rinsed at room temperature, they were probed with the appropriate secondary antibody. Images were captured with an Image Station 4000MM Pro (Carestream Health Inc., Woodbridge, MA, USA) and quantified using ImageJ software. The following primary antibodies were used: rabbit anti-AKT (#4691S, 1:1000, Cell Signaling Technology), rabbit anti-phospho-AKT (#13038S, 1:1000, Cell Signaling Technology), rabbit anti-PI3K (#4249S, 1:1000, Cell Signaling Technology), rabbit anti-phospho-PI3K (ab32401, 1:1000, Abcam), rabbit anti-mTOR (#2983, 1:1000, Cell Signaling Technology), rabbit anti-phospho-mTOR (#5536T, 1:1000, Cell Signaling Technology), rabbit anti-sequestosome 1 (#5114S, 1:1000, Cell Signaling Technology), rabbit anti-LC3B (#3868S, 1:1000, Cell Signaling Technology), rabbit anti-BCL2-associated X protein (BAX) (50599-1-Ig, 1:1000, Proteintech), rabbit anti-B-cell lymphoma 2 (BCL-2) (#3498S, 1:1000, Cell Signaling Technology).

Orthotopic xenograft model

P3 glioma cells expressing luciferase-GFP (1×10^6) in a total volume of 10 μL of serum-free Dulbecco's modified Eagle's medium were implanted into the right striatum of athymic mice (male; 4 weeks old; 20-30 g; OBiO Technology; Shanghai, China). Tumors visualized using bioluminescence imaging (PerkinElmer IVIS Spectrum; Waltham, MA, USA). The mice were subsequently divided into the following four groups: control; BZ; chloroquine (CQ; Sigma-Aldrich, C6628); and BZ + CQ. The mice were intraperitoneally injected with dimethyl sulfoxide alone (control), BZ (100 mg/kg/day), CQ (25 mg/kg/day), or BZ (100 mg/kg/day) + CQ (25 mg/kg/day). The tumor volumes were monitored using bioluminescence imaging, and the weight of each mouse was recorded weekly for 4 weeks. The tumor-bearing nude mice were treated until the onset of severe symptoms (a decrease of more than 10% in body weight or inability to return to an upright position after being pushed down) or death, at which point the experiment was terminated. Surviving mice were euthanized by intraperitoneal injection of sodium pentobarbital (150 mg/kg). Excised tumor tissues were snap-frozen in liquid nitrogen or fixed in formalin for further analysis.

Immunohistochemistry

Tumors were removed from sacrificed mice, fixed in 4% paraformaldehyde, and embedded in paraffin. Paraffin-embedded samples were

sectioned (4 μM), and the slides were then incubated with primary antibodies (rabbit anti-Ki67 1:200 dilution) at 4°C overnight, followed by incubation with a horseradish peroxidase-conjugated secondary antibody for 1 h at room temperature. Antibodies were detected using diaminobenzidine (Beyotime, Shanghai, China), and the slides were counterstained with hematoxylin (Beyotime, Shanghai, China).

Statistical analysis

Each assay was performed using GraphPad Prism 8.0 software. The results were presented as the mean ± standard deviation. The significance of the differences between groups was statistically analyzed by one-way analysis of variance followed by Tukey's test. All the experiments were repeated at least three times. Statistical significance was indicated in the figures as follows: $*P < 0.05$, $**P < 0.01$, and $***P < 0.001$.

Results

BZ inhibits the viability and proliferation of GBM cells

We investigated the effects of different concentrations of BZ on GBM cell growth using the P3 cell line (a representative primary GBM cell line), as well as LN229 and U251 cell lines (the most common laboratory GBM cell lines). The cell viability of the GBM cells was significantly inhibited after BZ treatment (40 μM), as determined by the xCELLigence RTCA eSight™ viability assay (**Figure 1A**). The results of the CCK-8 assay revealed that BZ inhibited the viability and proliferation of GBM cells relative to the controls in a time- and dose-dependent manner (**Figure 1B**). The IC_{50} values for U251, LN229, and P3 cells were 52.67, 52.29, and 24.84 μM at 24 h; 43.29, 37.87, and 20.94 μM at 48 h; and 26.76, 20.13, and 17.80 μM at 72 h, respectively. We chose LN229 and U251 for subsequent functional experiments. In addition, the EdU assay revealed that treatment with increasing concentrations of BZ significantly reduced GBM cell proliferation (**Figure 1C**, **1D**). Specifically, treatment with 20 μM BZ resulted in 56% and 64% decreases in U251 and LN229 cells, respectively, while treatment with 40 μM BZ resulted in 87% and 85% decreases, indicating that BZ inhibited GBM cell proliferation. In the colony formation assay, the number of colonies decreased by 44% for U251 cells and 58% for LN229 cells with 20 μM BZ, and decreased by 90% for U251 cells and 95% for LN229 cells with 40 μM BZ (**Figure 1E**, **1F**). These findings indicate that BZ is a promising agent for inhibiting GBM cell proliferation.

BZ inhibits the invasion and migration of GBM cells

Metastasis and invasion are challenges associated with tumor treatment [26]. To study whether BZ affects the invasion and migration of GBM cells, Transwell, 3D invasion, and wound healing assays was performed on BZ-treated GBM cells. The wound healing assay revealed that BZ-treated U251 and LN229 cells had significantly lower migration rates than untreated cells (**Figure 2A** and **2B**). In addition, as shown in **Figure 2C** and **2D**, the number of migrated U251 and LN229 cells decreased in a dose-dependent manner after 48 h of BZ treatment compared with the control groups. The number of U251 cells that invaded through the membrane decreased from 395 (0 μM BZ) to 139 (20 μM BZ) and to 39 (40 μM BZ) in the Transwell assays. Similarly, the number of LN229 cells decreased from more than 395 (0 μM BZ) to 184 (20 μM BZ) and to 35 (40 μM BZ). Furthermore, we examined the invasion capacity of U251 and LN229 cell spheroids in suspension culture through 3D invasion assays. After 96 h, the invasion distance of U251 spheres in Matrigel decreased to 62.5% and 32.6% of the control at 20 μM and 40 μM BZ, respectively. For LN229 cells, the invasion distance decreased to 14% of the control at 40 μM BZ (**Figure 2E** and **2F**). According to these data, BZ inhibited GBM cell invasion and migration in a dose-dependent manner.

Effects of BZ on GBM cell apoptosis in vitro

In the live/dead cell viability assay, the percentage of dead U251 glioma cells (red fluorescence) increased to 8% at 20 μM BZ and 29% at 40 μM BZ, compared with the control group. Similarly, the percentage of dead LN229 glioma cells (red fluorescence) increased to 12.2% at 20 μM BZ and 34.5% at 40 μM BZ, compared with the control group. The percentage of dead P3 glioma cells (red fluorescence) increased to 4.1% at 20 μM BZ and 15.4% at 40 μM BZ, compared with the control group (**Figure 3A** and **3B**). Additionally, to determine whether BZ

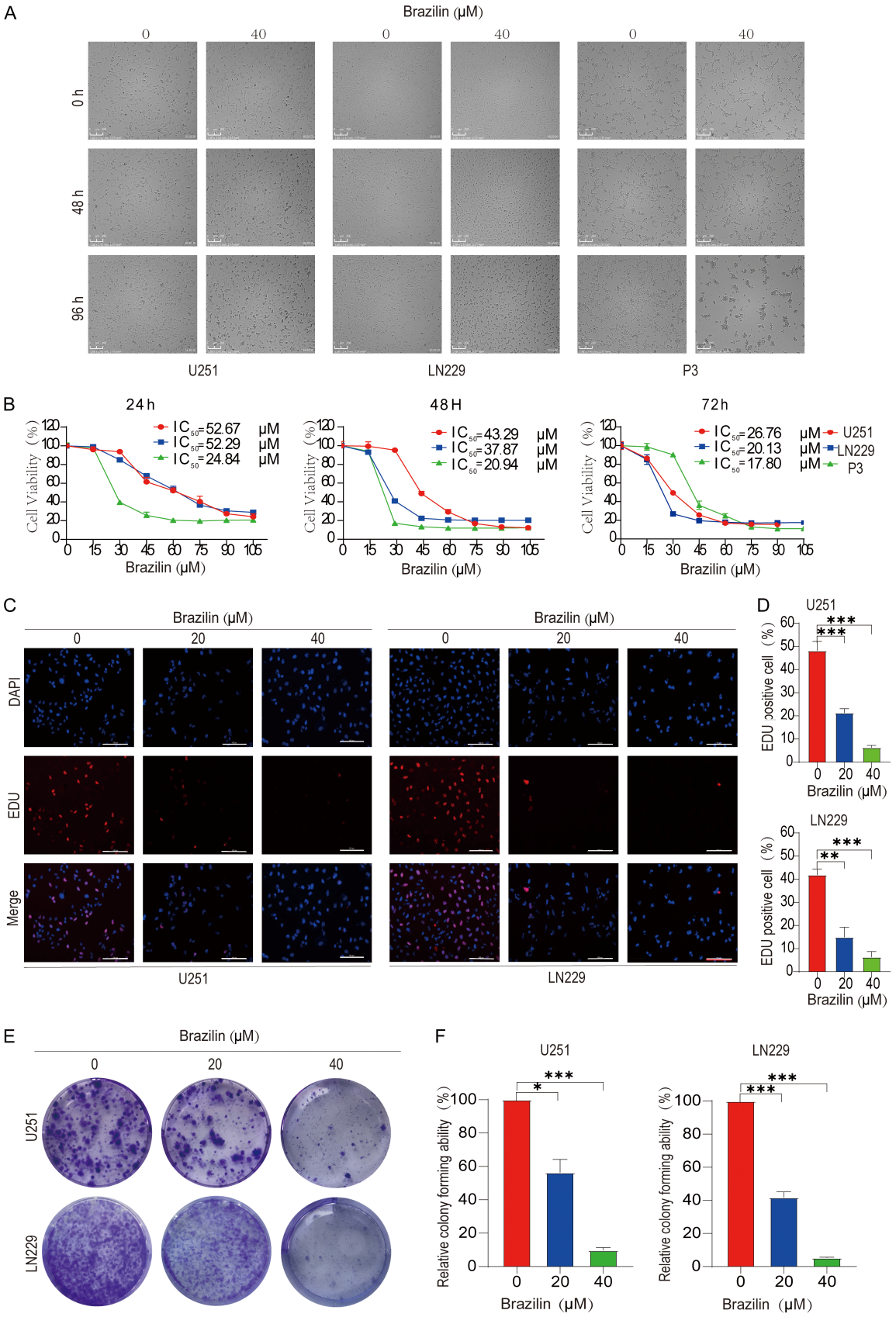
A
Brazilin (μM)
0
40
0 h
48 h
96 h
U251
LN229
P3
B
24 h
48 H
72 h
Cell Viability (%)
IC50=52.67 μM
IC50=52.29 μM
IC50=24.84 μM
IC50=43.29 μM
IC50=37.87 μM
IC50=20.94 μM
IC50=26.76 μM
IC50=20.13 μM
IC50=17.80 μM
U251
LN229
P3
Brazilin (μM)
C
Brazilin (μM)
0
20
40
DAPI
EDU
Merge
U251
LN229
D
U251
LN229
EDU positive cell (%)
Brazilin (μM)
E
Brazilin (μM)
U251
LN229
F
U251
LN229
Relative colony forming ability (%)
Brazilin (μM)

Figure 1. BZ inhibits the proliferation of GBM cells. A. Morphological changes of GBM cells treated with 40 μM BZ at 0, 48, and 96 h. B. Viability of GBM cells treated with different concentrations of BZ was assessed by the CCK-8 assay. C. Fluorescence images of EdU incorporation in U251 and LN229 cells treated with different concentrations of BZ for 48 h. Cells were stained with DAPI (blue) for nuclei and Apollo 567 (red) for EdU detection. Scale bars: 100 μM. D. Quantification of EdU-positive cells. E. Representative images of colony formation assays in U251 and LN229 cells treated with the indicated concentrations of BZ. F. Quantification of relative colony forming ability. *P < 0.05, **P < 0.01, and ***P < 0.001 compared with the control group. Brazilin (BZ), Cell counting kit-8 (CCK-8), 5-ethynyl-2'-deoxyuridine (EdU), 4',6-diamidino-2-phenylindole (DAPI), Glioblastoma (GBM).

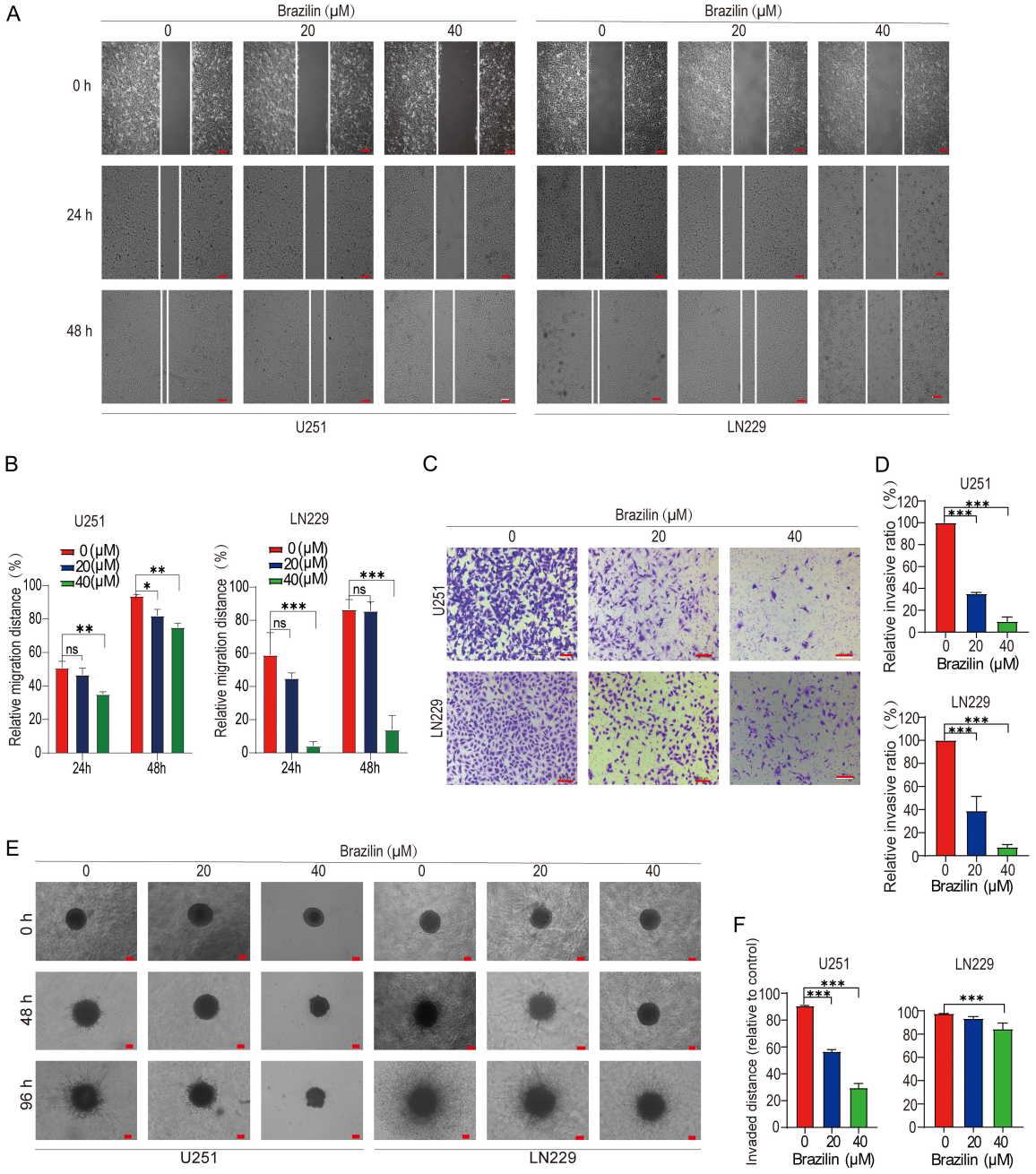

Figure 2. Different concentrations of BZ inhibited the migration and invasion of GBM cells *in vitro*. A, B. The wound healing assay was used to detected the migration of U251 and LN229 cells treated with BZ. Scale bars = 200 μM. C, D. The Transwell invasion assay was used to detect the invasion of GBM cells treated with BZ. Scale bars = 200 μM. E, F. The 3D invasion assay was used to evaluate the invasion capacity of GBM cells treated with different concentrations of BZ. Scale bars = 200 μM. ns, not significant, *P < 0.05, **P < 0.01, and ***P < 0.001 compared with the control group. Three-dimensional (3D), Brazilin (BZ), Glioblastoma (GBM).

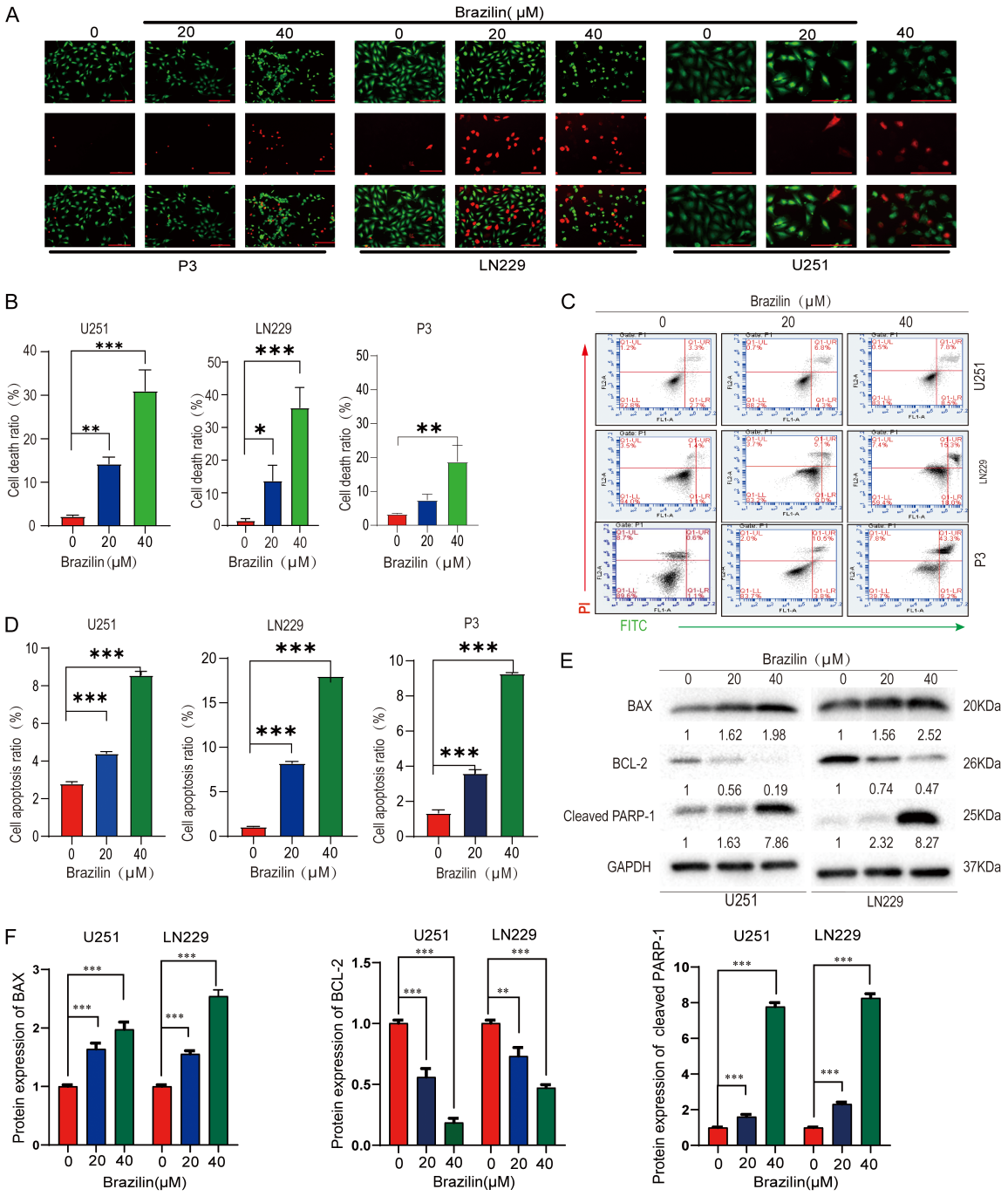

Figure 3. BZ induces apoptosis in GBM cells. A, B. Live (green)/dead (red) staining images of U251, LN229, and P3 cells treated with BZ. Scale bars = 200 μM. C, D. Annexin V-FITC and PI staining were used to evaluate apoptosis in GBM cells treated with BZ. E, F. WB analysis was used to detect the expression of apoptosis-related proteins (cleaved PARP-1, BCL-2, BAX) in GBM cells treated with BZ. *P < 0.05, **P < 0.01, and ***P < 0.001 compared with the control group. Annexin V-fluorescein isothiocyanate (V-FITC), Propidium iodide (PI), Poly (ADP-ribose) polymerase-1 (PARP-1), B-cell lymphoma 2 (BCL-2), BCL2-associated X protein (BAX), Glioblastoma (GBM), Brazilin (BZ), Western blot (WB), Glyceraldehyde-3-phosphate dehydrogenase (GAPDH).

could induce apoptosis, we analyzed U251, LN229, and P3 cells exposed to BZ for 48 h by flow cytometry. U251 cells exhibited apoptosis rates of 3.5% at 20 μM BZ and 4.5% at 40 μM BZ, compared with the control group. LN229 cells exhibited apoptosis rates of 3.7% at 20 μM BZ and 13.9% at 40 μM BZ, compared with the control group. P3 cells exhibited apoptosis

rates of 7.1% at 20 μM BZ and 39.9% at 40 μM BZ, compared with the control group (**Figure 3C** and **3D**). WB analysis was employed to investigate the role of BZ in apoptosis in GBM cells. The WB analysis showed increased expression of BAX and cleaved poly (ADP-ribose) polymerase-1 (PARP-1) and decreased expression of BCL-2 in cells treated with different concentrations of BZ (**Figure 3E** and **3F**). These findings suggest that BZ promotes apoptosis in GBM cells.

BZ induces autophagy in GBM cells in vitro

To examine the relationship between autophagy and BZ in GBM cells in vitro, we generated GBM cells with stable expression of a monomeric red fluorescent protein-GFP-LC3B dual-fluorescence reporter. The number of autophagosomes and autolysosomes obviously increased in U251 cells after BZ treatment (**Figure 4A** and **4B**). In addition, WB analysis was used to detect the expression of autophagy-related proteins. As indicated in **Figure 4C** and **4D**, BZ significantly increased the protein expression of LC3B-II and decreased the protein expression of sequestosome 1 in a dose-dependent manner. We further explored the mechanism of BZ-induced autophagy by using autophagy inhibitors. We cotreated GBM cells with BZ and autophagy inhibitors that block different phases of autophagy: early3-methyladenine (3-MA) for the early phase and CQ for the late phase. The effects were measured by WB analysis. These findings revealed that 3-MA or CQ treatment effectively reversed BZ-induced autophagy in U251 and LN229 cells (**Figure 4E-H**).

Autophagy inhibition enhances BZ-induced apoptosis in GBM cells

During programmed GBM cell death, the relationship between apoptosis and autophagy can be mutually exclusive or coordinated [27, 28]. Therefore, we investigated the relationship between apoptosis and autophagy in GBM cells treated with BZ. As determined by WB analysis, the expression of the pro-apoptotic proteins BAX and cleaved PARP-1 increased in BZ-treated U251 and LN229 cells in the presence of 3-MA or CQ, while the expression of the anti-apoptotic protein BCL-2 decreased (**Figure 5A-D**). Moreover, compared with cells treated with BZ alone, GBM cells coincubated with BZ plus 3-MA or CQ exhibited a higher rate of apoptosis (**Figure 5E** and **5F**). The EdU assay revealed a decrease in proliferation of GBM cells that were cotreated with 3-MA or CQ and BZ (**Figure 5G**). In addition, cells treated with 3-MA or CQ alone showed increased apoptosis rates and decreased proliferation. These findings suggest that autophagy inhibition may enhance BZ-induced apoptosis in GBM cells.

BZ may regulate the PI3K/AKT/mTOR signaling pathway in GBM cells

Autophagy is a complex biological process that is regulated by multiple pathways. The PI3K/AKT/mTOR signaling pathway is critical for autophagy and is closely associated with apoptosis and metabolism [29]. RNA sequencing revealed potential apoptosis- and autophagy-related protein targets of BZ in GBM cells (**Figure 6A**). To determine whether BZ regulates the PI3K/AKT/mTOR signaling pathway, the expression levels of proteins involved in this pathway were detected by WB analysis. In U251 and LN229 cells treated with BZ, the levels of phosphorylated PI3K, AKT, and mTOR decreased compared with those in the control groups (**Figure 6B** and **6C**).

BZ inhibits the growth of GBM cells in vivo

P3 cells with stable luciferase expression were inoculated into the brains of athymic mice. Tumor growth was monitored using luciferase bioluminescence imaging. Compared with vehicle treatment, BZ treatment significantly inhibited tumor growth in mice (**Figure 7A** and **7B**). At 3 weeks, the bioluminescence signals were approximately 2.6×10^8 photons/s in the control group, 1.1×10^8 photons/s in the CQ group, 0.4×10^8 photons/s in the BZ group, and 0.3×10^8 photons/s in the CQ + BZ group. Immunohistochemical staining was used to examine the expression of Ki67. Consistent with the in vivo experi-mental results, we found that co-treatment with 3-MA or CQ and BZ inhibited proliferation in GBM tumor tissues (**Figure 7C**). Taken together, these findings suggested that BZ suppressed tumor growth in vivo and that combined treatment with an inhibitor of autophagy enhanced BZ-induced tumor growth inhibition.

Discussion

GBM is one of the most common intracranial malignancies in neurosurgery, accounting for

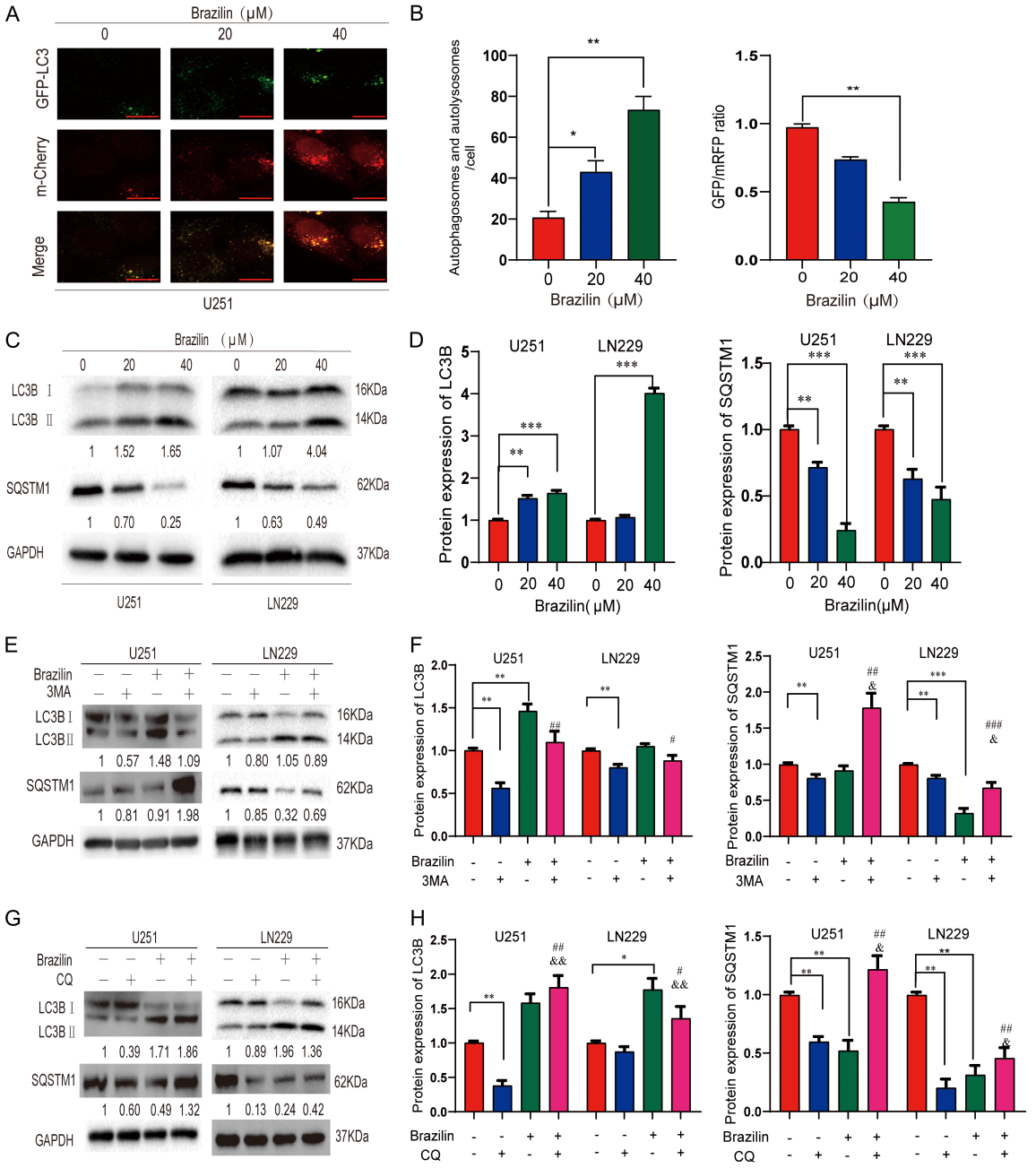

Figure 4. BZ induces autophagy in GBM cells in vitro. A, B. The distribution of GFP-mCherry-LC3B in U251 cells was observed under an inverted fluorescence microscope. Merged red and green fluorescence (yellow) represented autophagosomes, while red fluorescence represented autolysosomes. The number of yellow and red puncta reflected the level of autophagy. Scale bars = 20 μM. C, D. WB analysis of lysates (20 μg) was performed to measure the levels of SQSTM1 and LC3B in GBM cells after treatment with BZ. E-H. WB analysis was performed to measure the levels of SQSTM1 and LC3B in GBM cells processed with 3-MA or CQ followed by exposure to BZ. Compared with control group, $^{*}P < 0.05$, $^{**}P < 0.01$, and $^{***}P < 0.001$. Compared with BZ group, $^{\#}P < 0.05$, $^{\#\#}P < 0.01$, and $^{\#\#\#}P < 0.001$. Compared with 3-MA or CQ group, $^{\&}P < 0.05$, $^{\&\&}P < 0.01$. Glioblastoma (GBM), Brazilin (BZ), Green fluorescent protein (GFP), Monomeric red fluorescent protein (mRFP), Light chain 3B (LC3B), Sequestosome 1 (SQSTM1), 3-methyladenine (3-MA), chloroquine (CQ), Western blot (WB), Glioblastoma (GBM), Glyceraldehyde-3-phosphate dehydrogenase (GAPDH).

50% to 60% of intracranial tumors [30]. GBM are the central nervous system malignant tumors with the highest incidence and mortality rates. Although current treatment methods

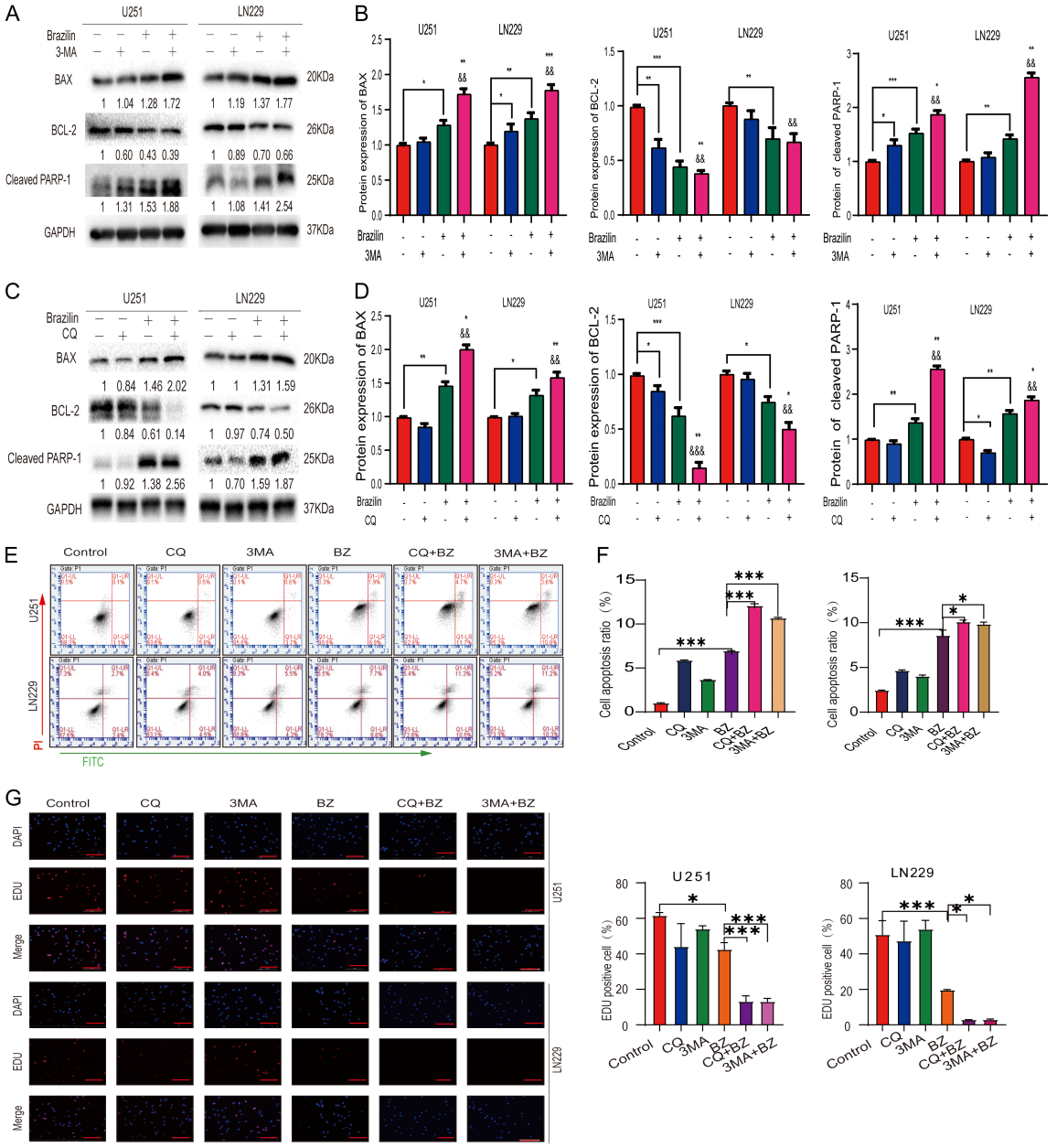

Figure 5. Autophagy inhibition enhances BZ-induced apoptosis in GBM cells. (A-D) WB analysis was performed to measure the levels of apoptosis-related proteins in GBM cells pretreated with with 3-MA (A, B) or CQ (C, D), followed by exposure to different concentrations of BZ. (E, F) Annexin V-FITC/PI staining was used to determine apoptosis rates in GBM cells pretreated with 3-MA or CQ and then treated with different concentrations of BZ. (G) EdU incorporation was assessed in GBM cells treated with 3-MA or CQ, followed by exposure to different concentrations of BZ. Scale bars = 100 μM. Compared with control group, $^{*}P < 0.05$, $^{**}P < 0.01$, and $^{***}P < 0.001$. Compared with 3-MA or CQ group, $^{\&\&}P < 0.01$, $^{\&\&\&}P < 0.001$. BCL2-associated X protein (BAX), B-cell lymphoma 2 (BCL-2), Poly (ADP-ribose) polymerase-1 (PARP-1), Glyceraldehyde-3-phosphate dehydrogenase (GAPDH), Glioblastoma (GBM), Brazilin (BZ), Western blot (WB), 3-methyladenine (3-MA), Chloroquine (CQ), Annexin V-fluorescein isothiocyanate (V-FITC), Propidium iodide (PI), 5-ethynyl-2'-deoxyuridine (EdU), 4',6-diamidino-2-phenylindole (DAPI).

can improve patient survival rates, the overall prognosis remains poor. Therefore, finding therapeutic targets and mechanisms for glioma is of great significance for developing effective new drugs.

Cancer is a complex disease that requires multifaceted treatment strategies, including the ability to inhibit cancer cell proliferation, induce differentiation and apoptosis [31], suppress cell invasion and migration by inhibiting regula-

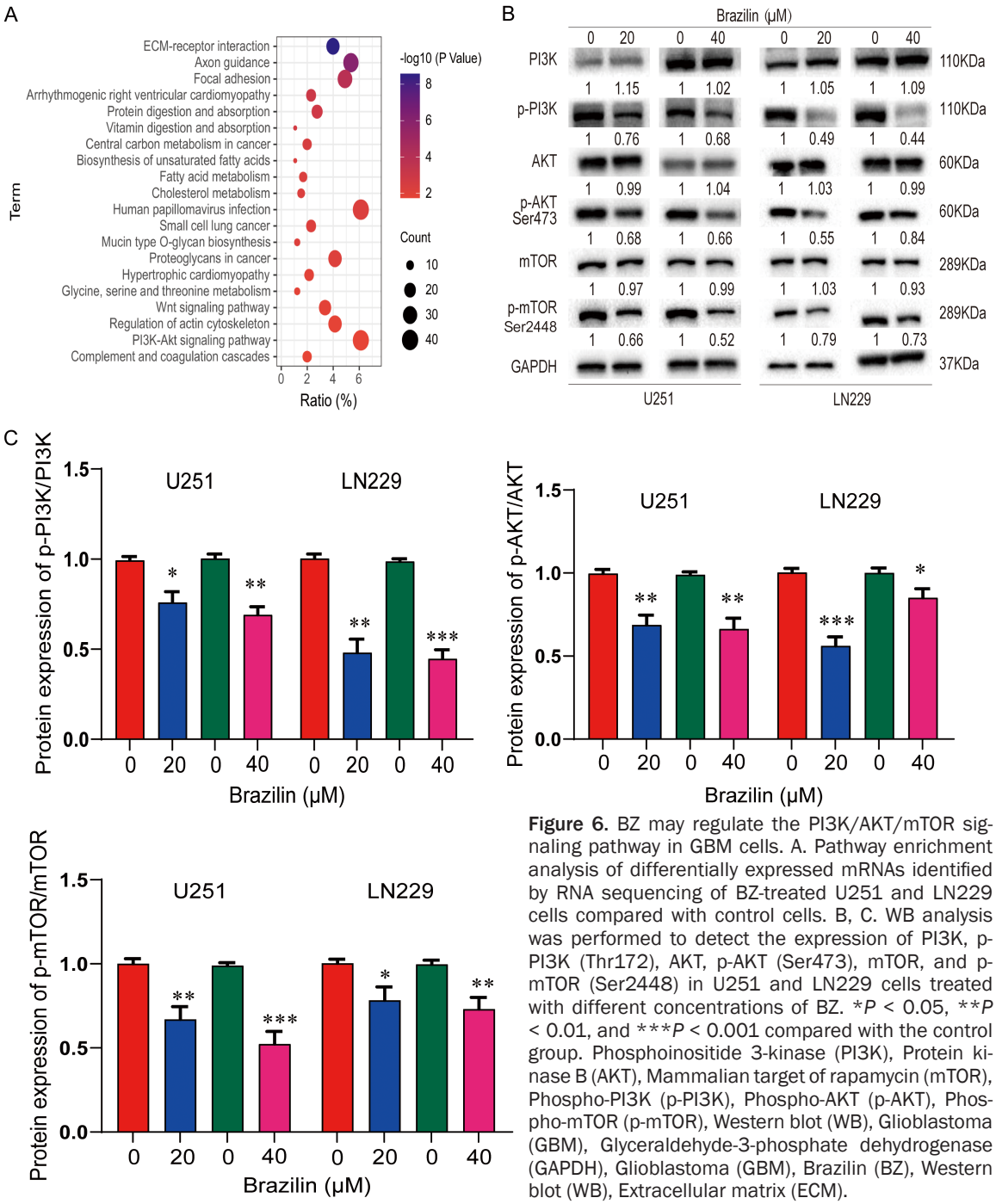

Figure 6. BZ may regulate the PI3K/AKT/mTOR signaling pathway in GBM cells. A. Pathway enrichment analysis of differentially expressed mRNAs identified by RNA sequencing of BZ-treated U251 and LN229 cells compared with control cells. B, C. WB analysis was performed to detect the expression of PI3K, p-PI3K (Thr172), AKT, p-AKT (Ser473), mTOR, and p-mTOR (Ser2448) in U251 and LN229 cells treated with different concentrations of BZ. $*P < 0.05$, $**P < 0.01$, and $***P < 0.001$ compared with the control group. Phosphoinositide 3-kinase (PI3K), Protein kinase B (AKT), Mammalian target of rapamycin (mTOR), Phospho-PI3K (p-PI3K), Phospho-AKT (p-AKT), Phospho-mTOR (p-mTOR), Western blot (WB), Glioblastoma (GBM), Glyceraldehyde-3-phosphate dehydrogenase (GAPDH), Glioblastoma (GBM), Brazilin (BZ), Western blot (WB), Extracellular matrix (ECM).

tory proteins [32], and target the cell cycle to block proliferation [33]. The elimination of cancer cells from the body through apoptosis is the final goal of treatment strategies. BZ, an active isoflavonoid compound derived from Chinese herbs, has displayed anti-cancer properties across various cancer cell lines [34]. BZ has been reported to have biological activities, including neuroprotective, hepatoprotective, antioxidant, anti-inflammatory, apoptotic induction, and anticancer effects [35, 36]. BZ inhibits proliferation and induces apoptosis in several cancer cell lines, including MCF-7 breast cancer [37], T24 urinary bladder cancer [9], U266 multiple myeloma [38], Cal27 head and neck squamous cell carcinoma [39], MG-63 osteosarcoma [25], and Tca8113 tongue cancer cells [24]. In the present study, using CCK-8, colony for-

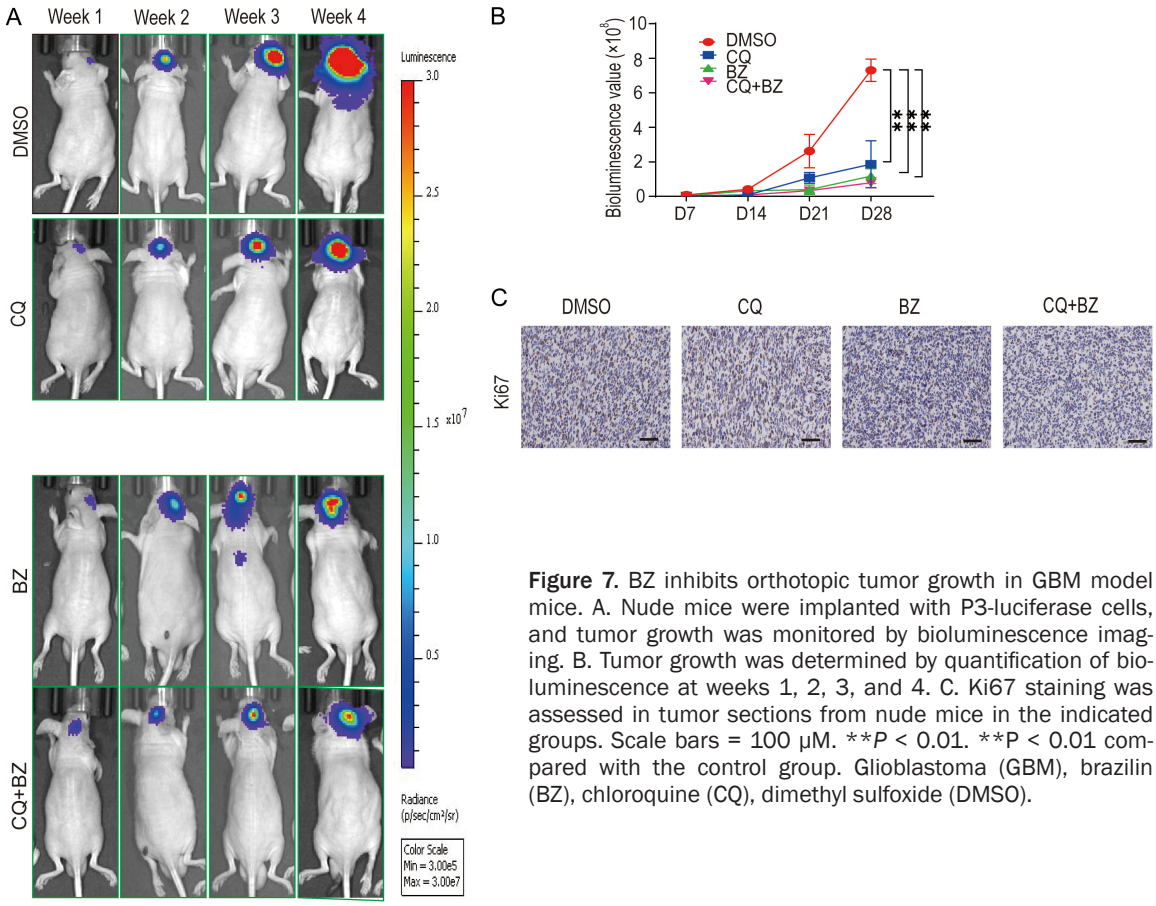

Figure 7. BZ inhibits orthotopic tumor growth in GBM model mice. A. Nude mice were implanted with P3-luciferase cells, and tumor growth was monitored by bioluminescence imaging. B. Tumor growth was determined by quantification of bioluminescence at weeks 1, 2, 3, and 4. C. Ki67 staining was assessed in tumor sections from nude mice in the indicated groups. Scale bars = 100 μM. $^{**}P < 0.01$. **P < 0.01 compared with the control group. Glioblastoma (GBM), brazilin (BZ), chloroquine (CQ), dimethyl sulfoxide (DMSO).

mation, flow cytometry, 3D invasion, live/dead, wound healing, and Transwell assays, we confirmed that BZ inhibited GBM cell viability and induced apoptosis. Apoptosis is a process by which cells die in an independent and controlled manner to maintain a stable internal environment [40, 41]. Therefore, inducing apoptosis in GBM cells may be a promising cancer treatment strategy [42]. Furthermore, we examined whether BZ-induced GBM cell death occurred through apoptosis and assessed the expression of BAX, BCL-2, and cleaved PARP-1 by WB analysis. The results revealed that BZ increased the expression of BAX and cleaved PARP-1 but suppressed the expression of BCL-2 in a dose-dependent manner. BAX increases the release of cytochrome c into the cytoplasm and ultimately initiates the formation of apoptosomes [43]. The above results indicated that BZ induced apoptosis in GBM cells in vitro.

Autophagy plays a role in the development and occurrence in malignant tumors [15]. Autophagy also plays a dual role in tumor suppression and promotion [44], but the relationship between BZ and autophagy has not been reported. LC3B is among the key proteins involved in the process of autophagy. We hypothesized that BZ leads to GBM cell death through the induction of autophagy. In this study, we observed that the BZ treatment resulted in more yellow puncta (autophagosomes) and red puncta (autolysosomes) in GBM cells in a dose-dependent manner. The results of WB analysis revealed that autophagosomes accumulated in GBM cells after BZ treatment. The administration of 3-MA or CQ reversed the activation of autophagy induced by BZ treatment. While our findings demonstrate the regulatory role of BZ in autophagy, the precise molecular mechanisms underlying its control of lysosomal homeostasis remain to be fully elucidated. Finally, using the autophagy inhibitors 3-MA and CQ, we found that the expression of autophagy- and apoptosis-related proteins was partially reversed following BZ treatment in GBM cells. Moreover, compared with cells treated with BZ alone, GBM cells co-incubated with BZ plus

3-MA or CQ exhibited a higher rate of apoptosis and a decrease in proliferation. These findings suggest that autophagy inhibition may enhance BZ-induced apoptosis in GBM cells.

In many cancers, the PI3K/AKT/mTOR signaling pathway plays important roles in the cell cycle, apoptosis, and autophagy [45]. RNA sequencing revealed potential apoptosis- and autophagy-related protein targets of BZ in GBM cells. In U251 and LN229 cells treated with BZ, the levels of phosphorylated PI3K, AKT, and mTOR decreased compared with those in the control groups, which suggested that BZ can inhibit the activation of the PI3K/AKT/mTOR signaling pathway in GBM cells. BZ may affect GBM tumor behavior by regulating the PI3K/AKT/mTOR pathway, but the specific mechanism underlying this regulation require further study.

Conclusion

To summarize, BZ exerts cancer-suppressive effects in GBM, which may be related to the PI3K/AKT/mTOR pathway. These results may provide a breakthrough for the treatment of GBM.

Acknowledgements

This article was supported by the Key R&D Program of Shandong Province (2025CXPT177) and the Shandong Provincial Laboratory Project (SYS202202).

Disclosure of conflict of interest

None.

Address correspondence to: Xingang Li, Department of Neurosurgery, Qilu Hospital, Cheeloo College of Medicine and Institute of Brain and Brain-Inspired Science, Shandong University, No. 107 Wenhua Xi Road, Jinan 250012, Shandong, P. R. China. Tel: +86-0531-82166615; Fax: +86-0531-82166615; E-mail: lixg@sdu.edu.cn

References

[1] Pouyan A, Ghorbanlo M, Eslami M, Jahanshahi M, Ziaei E, Salami A, Mokhtari K, Shahpasand K, Farahani N, Meybodi TE, Entezari M, Taheriazam A, Hushmandi K and Hashemi M. Glioblastoma multiforme: insights into pathogenesis, key signaling pathways, and therapeutic strategies. Mol Cancer 2025; 24: 58.

[2] Bou-Gharios J, Noël G and Burckel H. The neglected burden of chronic hypoxia on the resistance of glioblastoma multiforme to first-line therapies. BMC Biol 2024; 22: 278.

[3] Alexopoulos G, Zhang J, Karampelas I, Patel M, Kemp J, Coppens J, Mattei TA and Mercier P. Long-term time series forecasting and updates on survival analysis of glioblastoma multiforme: a 1975-2018 population-based study. Neuroepidemiology 2022; 56: 75-89.

[4] Wu M, Miska J, Xiao T, Zhang P, Kane JR, Balyasnikova IV, Chandler JP, Horbinski CM and Lesniak MS. Race influences survival in glioblastoma patients with KPS ≥ 80 and associates with genetic markers of retinoic acid metabolism. J Neurooncol 2019; 142: 375-384.

[5] Xie XP, Ganbold M, Li J, Lien M, Chipman ME, Wang T, Jayewickreme CD, Pedraza AM, Bale T, Tabar V, Brennan C, Sun D, Sharma R and Parada LF. Glioblastoma functional heterogeneity and enrichment of cancer stem cells with tumor recurrence. Neuron 2024; 112: 4017-4032, e4016.

[6] Zhao J, Zhang L, Mu F, Yu Y, Cui C, Tang M, Sun K, Yin Y, Wang J and Gong R. Brazilin attenuates kidney ischemia-reperfusion injury by regulating inflammation, oxidative stress, and mitochondrial dysfunction. Histol Histopathol 2026; 41: 673-689.

[7] Li S, Wang K, Jiang K, Xing D, Deng R, Xu Y, Ding Y, Guan H, Chen LL, Wang D, Chen Y, Bu W and Xiang Y. Brazilin-Ce nanoparticles attenuate inflammation by de/anti-phosphorylation of IKKbeta. Biomaterials 2024; 305: 122466.

[8] Rojas EM, Zhang H, Velu SE and Wu H. Tetracyclic homoisoflavanoid (+)-brazilin: a natural product inhibits c-di-AMP-producing enzyme and Streptococcus mutans biofilms. Microbiol Spectr 2024; 12: e0241823.

[9] Yang X, Zhang S, He J, Zhao L, Chen L, Yang Y, Wang J, Yan L and Zhang T. Brazilin inhibits bladder cancer by promoting cell necroptosis. Clin Exp Pharmacol Physiol 2023; 50: 738-748.

[10] Li ZY, Zheng Y, Chen Y, Pan M, Zheng SB, Huang W, Zhou ZH and Ye HY. Brazilin ameliorates diabetic nephropathy and inflammation in db/db mice. Inflammation 2017; 40: 1365-1374.

[11] Cui Z, Guo FY, Li L, Lu F, Jin CH, Wang X and Liu F. Brazilin-7-acetate, a novel potential drug of Parkinson's disease, hinders the formation of alpha-synuclein fibril, mitigates cytotoxicity, and decreases oxidative stress. Eur J Med Chem 2024; 264: 115965.

[12] Yan X, Xu L, Qi C, Chang Y, Zhang J, Li N, Shi B, Guan B, Hu S, Huang C, Wang H, Chen Y, Xu X,

Lu J, Xu G, Chen C, Li S and Chen Y. Brazilin alleviates acute lung injury via inhibition of ferroptosis through the SIRT3/GPX4 pathway. Apoptosis 2025; 30: 768-783.
[13] Ariosa AR, Lahiri V, Lei Y, Yang Y, Yin Z, Zhang Z and Klionsky DJ. A perspective on the role of autophagy in cancer. Biochim Biophys Acta Mol Basis Dis 2021; 1867: 166262.
[14] Li X, He S and Ma B. Autophagy and autophagy-related proteins in cancer. Mol Cancer 2020; 19: 12.
[15] Niu X, You Q, Hou K, Tian Y, Wei P, Zhu Y, Gao B, Ashrafizadeh M, Aref AR, Kalbasi A, Cañadas I, Sethi G, Tergaonkar V, Wang L, Lin Y, Kang D and Klionsky DJ. Autophagy in cancer development, immune evasion, and drug resistance. Drug Resist Updat 2025; 78: 101170.
[16] Nie T, Zhu L and Yang Q. The classification and basic processes of autophagy. Adv Exp Med Biol 2021; 1208: 3-16.
[17] Yamamoto H and Matsui T. Molecular mechanisms of macroautophagy, microautophagy, and chaperone-mediated autophagy. J Nippon Med Sch 2024; 91: 2-9.
[18] Fleming A, Bourdenx M, Fujimaki M, Karabiyik C, Krause GJ, Lopez A, Martín-Segura A, Puri C, Scrivo A, Skidmore J, Son SM, Stamatakou E, Wrobel L, Zhu Y, Cuervo AM and Rubinsztein DC. The different autophagy degradation pathways and neurodegeneration. Neuron 2022; 110: 935-966.
[19] Zhou C, Wu Z, Du W, Que H, Wang Y, Ouyang Q, Jian F, Yuan W, Zhao Y, Tian R, Li Y, Chen Y, Gao S, Wong CCL and Rong Y. Recycling of autophagosomal components from autolysosomes by the recycler complex. Nat Cell Biol 2022; 24: 497-512.
[20] Lőrincz P and Juhász G. Autophagosome-lysosome fusion. J Mol Biol 2020; 432: 2462-2482.
[21] Liu S, Yao S, Yang H, Liu S and Wang Y. Autophagy: regulator of cell death. Cell Death Dis 2023; 14: 648.
[22] Denton D and Kumar S. Autophagy-dependent cell death. Cell Death Differ 2019; 26: 605-616.
[23] Dong Q, Wang D, Li L, Wang J, Li Q, Duan L, Yin H, Wang X, Liu Y, Yuan G and Pan Y. Biochanin A sensitizes glioblastoma to temozolomide by inhibiting autophagy. Mol Neurobiol 2022; 59: 1262-1272.
[24] Jia Y, Tong X and Fan J. Effect of brazilin on apoptosis and autophagy of tongue cancer Tca8113 cells and its molecular mechanism. Nan Fang Yi Ke Da Xue Xue Bao 2019; 39: 351-356.
[25] Kang Y, He P, Wang H, Ye Y, Li X, Xie P and Wu B. Brazilin induces FOXO3A-dependent autophagic cell death by disturbing calcium homeostasis in osteosarcoma cells. Cancer Chemother Pharmacol 2018; 82: 479-491.
[26] Li Y, Liu F, Cai Q, Deng L, Ouyang Q, Zhang XH and Zheng J. Invasion and metastasis in cancer: molecular insights and therapeutic targets. Signal Transduct Target Ther 2025; 10: 57.
[27] Chen J, Rodriguez AS, Morales MA and Fang X. Autophagy modulation and its implications on glioblastoma treatment. Curr Issues Mol Biol 2023; 45: 8687-8703.
[28] Christoff M, Szczepańska A, Jakubowicz-Gil J and Zajac A. Reprogramming the apoptosis-autophagy axis in glioblastoma: the central role of the Bcl-2:Beclin-1 complex and survival signalling networks. Cells 2025; 15: 53.
[29] Hwang YK, Lee DH, Lee EC and Oh JS. Importance of autophagy regulation in glioblastoma with temozolomide resistance. Cells 2024; 13: 1332.
[30] Fan H, Xie X, Kuang X, Du J and Peng F. MicroRNAs, key regulators in glioma progression as potential therapeutic targets for Chinese medicine. Am J Chin Med 2022; 50: 1799-1825.
[31] He J, Zhang L, Xu H, Gao C, Zhao W, Zhang B, Han W, Zhao W, Tan G, Chen S, Zhong P, Shen Z, Meng J, Tang Z, Lu H, Gao X, Li Z, Li W, Mao J, Liu B, Zhang YW and Wang Z. CSRP2 promotes the glioblastoma mesenchymal phenotype via p130Cas-mediated NF-kappaB and MAPK pathways. J Exp Clin Cancer Res 2025; 44: 228.
[32] Liu Y, Ni K, Zhao S, Zhao J, Zhong M, Cheng C, Ji W, Jiao J and Shao J. CBLB regulates MAPK-P38 pathway via MAP3K9 ubiquitination to inhibit GBM cell invasion and migration. J Cell Physiol 2025; 240: e70037.
[33] Xi Y, Yang Q, Wang Y, An W, Huang X, Sun C, Luo W, Shi C, Wang Q, Pan H, Chen Q, Li X, Hua D, Yu S and Zhou X. ZNRF2 is essential for gliomagenesis through orchestrating glycolysis and acts as a promising therapeutic target in glioma. J Transl Med 2025; 23: 185.
[34] Kang LP, Xu C, Xu P, Huang DH and Jiang ZB. Brazilin inhibits the proliferation of non-small cell lung cancer by regulating the STING/TBK1/IRF3 pathway. J Cell Mol Med 2025; 29: e70688.
[35] Raptania CN, Zakia S, Fahira AI and Amalia R. Article review: brazilin as potential anticancer agent. Front Pharmacol 2024; 15: 1355533.
[36] Nava-Tapia DA, Cayetano-Salazar L, Herrera-Zúñiga LD, Bello-Martínez J, Mendoza-Catalán MA and Navarro-Tito N. Brazilin: biological activities and therapeutic potential in chronic degenerative diseases and cancer. Pharmacol Res 2022; 175: 106023.
[37] Cayetano-Salazar L, Hernandez-Moreno JA, Bello-Martinez J, Olea-Flores M, Castañeda-

Saucedo E, Ramirez M, Mendoza-Catalán MA and Navarro-Tito N. Regulation of cellular and molecular markers of epithelial-mesenchymal transition by Brazilin in breast cancer cells. PeerJ 2024; 12: e17360.

[38] Kim B, Kim SH, Jeong SJ, Sohn EJ, Jung JH, Lee MH and Kim SH. Brazilin induces apoptosis and G2/M arrest via inactivation of histone deacetylase in multiple myeloma U266 cells. J Agric Food Chem 2012; 60: 9882-9889.

[39] He ZJ, Zhu FY, Li SS, Zhong L, Tan HY and Wang K. Inhibiting ROS-NF-kappaB-dependent autophagy enhanced brazilin-induced apoptosis in head and neck squamous cell carcinoma. Food Chem Toxicol 2017; 101: 55-66.

[40] Morana O, Wood W and Gregory CD. The apoptosis paradox in cancer. Int J Mol Sci 2022; 23: 1328.

[41] Singh P and Lim B. Targeting apoptosis in cancer. Curr Oncol Rep 2022; 24: 273-284.

[42] Wang W, Yuan X, Mu J, Zou Y, Xu L, Chen J, Zhu X, Li B, Zeng Z, Wu X, Yin Z and Wang Q. Quercetin induces MGMT+ glioblastoma cells apoptosis via dual inhibition of Wnt3a/beta-Catenin and Akt/NF-kappaB signaling pathways. Phytomedicine 2023; 118: 154933.

[43] Wang H, Zhou HC, Ren RL, Du SX, Guo ZK and Shen XH. Apolipoprotein E2 inhibits mitochondrial apoptosis in pancreatic cancer cells through ERK1/2/CREB/BCL-2 signaling. Hepatobiliary Pancreat Dis Int 2023; 22: 179-189.

[44] Rangel M, Kong J, Bhatt V, Khayati K and Guo JY. Autophagy and tumorigenesis. FEBS J 2022; 289: 7177-7198.

[45] Yu L, Wei J and Liu P. Attacking the PI3K/Akt/mTOR signaling pathway for targeted therapeutic treatment in human cancer. Semin Cancer Biol 2022; 85: 69-94.